Experimentally Determined Thermochemical Properties of the Malonic Acid/Water System: Implications for Atmospheric Aerosols

Anne R. Hansen and Keith D. Beyer*

Department of Chemistry, Wisconsin Lutheran College, 8800 W. Bluemound Road, Milwaukee, Wisconsin 53226

Received: November 26, 2003; In Final Form: February 13, 2004

The liquid/solid phase diagram, solution heat capacities, water activities, enthalpies of fusion, and eutectic temperature of the malonic acid/water binary system have been investigated using differential scanning calorimetry and infrared (IR) spectroscopy of thin films. We report here measurements of the ice melting envelope, malonic acid dissolution envelope, and the ice/malonic acid eutectic temperature and composition in this binary system. We also report the first observation of a malonic acid hydrate, possibly $C_3H_4O_4 \cdot 6H_2O$, using both thermal analysis and IR spectroscopy. We have observed the formation of this hydrate over a large range of concentrations and determined that it can be a significant fraction of samples within that region. We have also determined the enthalpy of fusion of malonic acid, as well as the constant pressure heat capacities of solutions in the concentration range of 5−55 wt % malonic acid from 323 K down to the freezing point of each solution. Water activities have also been determined using the freezing point depression of ice. We compare our results to those recently reported in the literature for bulk solutions and aerosols.

1. Introduction

Recent field measurements have shown that organic material may be present in many tropospheric aerosols.[1−4] In fact, Murphy et al.[5] reported observations that aerosols in the upper troposphere may contain more organic material than sulfate. Studies have shown that the incorporation of organic compounds into ammonium sulfate aerosols changes their deliquescence, efflorescence, and hygroscopic properties, and potentially their crystallization properties.[6−8] This necessitates understanding the impact of organic substances on the phase transitions of aqueous systems that comprise tropospheric aerosols. Some of the most abundant organic compounds found in aerosols are the dicarboxylic acids (oxalic acid, malonic acid, glutaric acid, etc.[9,10]). In this study, we have focused on the thermodynamics of the malonic acid/water system.

Some work has been performed in regard to studying the properties of solid malonic acid,[11,12] which is useful in understanding the aqueous system. With respect to the aqueous system, the temperature dependent solubilities of malonic acid have been known at concentrations of 50 wt % and higher.[13] These values have recently been confirmed via the study of bulk solutions,[8,14,15] with Braban et al.[15] performing the first measurements of the ice-melting envelope in this system. Work has also been done on aerosol deliquescence and efflorescence relative humidities, which leads to determination of water activities in this system, where the aerosol water concentration is directly measured.[16−19] Heat capacity measurements at 303 K have also been performed for very dilute solutions.[20] In the experiments described here, we have taken a different experimental approach than those previously cited. We have undertaken a study of the malonic acid/water phase diagram, enthalpies of fusion, water activities, and solution heat capacities over a wide concentration range and at subambient temperatures using thermal analysis and Fourier transform infrared (FTIR) spectroscopy of thin films.

2. Experimental Section

2.1. Sample Preparation. Samples were prepared by dissolving 99%+ pure ACS reagent-grade $C_3H_4O_4$ (formula weight of 104.06 g/mol) supplied by Aldrich with Culligan purified water. The concentrations of all samples were known to within ±0.005 wt %.

2.2. Infrared Spectra. The sample cell used for infrared (IR) spectra has been shown schematically and explained in detail in previous literature.[21] Briefly, a small drop of malonic acid solution was placed between two AgCl windows, which were held in the center of an aluminum block by a threaded metal ring. Sample volumes were ∼2 μL. On each side of the aluminum block, a Pyrex cell was purged with dry nitrogen gas. KBr windows were placed on the end of each cell, sealed with O-rings, and held in place by metal clamps. Heat tape was wrapped around the purge cells to prevent condensation on the KBr windows. The sample was cooled by immersing the end of the aluminum block in liquid nitrogen and warmed by resistive heaters connected to a temperature controller. Temperature was measured by a copper/constantan thermocouple placed at the edge of the AgCl windows and connected to the temperature controller. The temperature of the cell was calibrated using Culligan purified water and high purity organic solvents (from Aldrich), including decane, octane, and acetic anhydride (the melting points of which are 243.5, 216.4, and 200.2 K, respectively[22]). The IR cell temperatures are known, on average, to within ±1.8 K of the transition temperatures measured with the differential scanning calorimeter (DSC).

Spectra were obtained using a spectrometer (Mattson Instruments, model Galaxy 4020 FTIR) with a resolution of 16 cm^{-1}. Each spectrum was the average of four scans. Before spectra

* Author to whom correspondence should be addressed. E-mail address: Keith_Beyer@wlc.edu.

10.1021/jp0376166 CCC: $27.50
Published on Web 03/26/2004

of a sample were taken, a reference scan was obtained from a dry, purged sample cell. Samples were cooled to 220 K at a rate of 3 K/min and then allowed to warm to or above room temperature without the use of resistive heating; typically, this occurred at a rate of ~1 K/min.

To obtain a spectrum of solid malonic acid, two methods were used. In one case, ~1 g of malonic acid was dissolved in 2.5 mL of methanol and allowed to dry on an AgCl window. A thin, papery film formed on the window, which was then placed in the FTIR and a spectrum was acquired. In the second method, a small amount of malonic acid solid was placed in a Pike Technologies ZnSe attenuated total reflectance (ATR) accessory, and the spectrum was acquired. Both spectra agreed well with literature references.[23−25]

2.3. Differential Scanning Calorimetry. Thermal data were obtained with a Mettler-Toledo model DSC 822e calorimeter with liquid nitrogen cooling. Industrial grade nitrogen gas was used to purge the instrument with a flow rate of 50.0 mL/min. The temperature reproducibility of this instrument is better than ±0.05 K. Our accuracy was estimated to be ±0.9 K, with a probability of 0.94, based on a three point temperature calibration[26] using indium, high performance liquid chromatography (HPLC) grade water, and anhydrous, high purity (99%+) octane from Aldrich, both stored under nitrogen. The sensitivity of our instrument to thermal signals is high. Previously, we have calculated our sensitivity to detecting a component undergoing a thermal transition to be <50 ppm.[27]

2.3.1. Phase Diagram Work. Samples were sealed in a 40 μL aluminum pan and typically had a mass of ~22 mg. A typical sample was cooled to 183 K at 10 K/min, held at 183 K for 5 min, warmed to 235 K at a rate of 10 K/min, held at 235 K for 5 min, and then finally warmed at a rate of 1 K/min to 298 K. For samples with >55 wt % malonic acid, the samples were warmed to 320 K at a rate of either 1 K/min or 5 K/min, to allow for the dissolution transition.

2.3.2. Heat Capacity Experiments. Samples (volume of 5 μL) were sealed in a 40 μL aluminum pan, with the sample in contact only with the bottom of the pan (not touching the walls). The cooling program consisted of a 2 min isothermal hold at 333 K, followed by cooling at 10 K/min to 183 K, and the process was completed by a 2 min isothermal hold at 183 K. The thermal effects of the aluminum pan were removed by subtracting the thermogram of an empty 40 μL aluminum pan from each sample and reference thermogram, respectively. We followed the method for measurement of heat capacity by DSC given in ASTM E 1269-01.[28] The reference material for this method is synthetic sapphire, which was supplied by Mettler-Toledo.

3. Results

3.1. Phase Diagram. The phase diagram of the malonic acid/water system is shown in Figure 1. In addition to our data, we have plotted the bulk solubility and freezing point data from the literature. Data from our DSC experiments that have been used to construct the phase diagram are given in Table 1. Our data are in excellent agreement with the literature work over a broad range of compositions. We have determined the melting of 99%+ pure malonic acid, using DSC, to be 407.46 ± 0.29 K, which is in good agreement with the literature value of 408.75 K.[29] We parametrized our data according to second order polynomial equations of the form

$$T = A_2X^2 + A_1X + A_0 \qquad (1)$$

where T is the melting temperature (in Kelvin), X is the water concentration (in wt %), and the A_i terms are the respective polynomial coefficients. We then utilized these equations to calculate both our experimental data and the literature data. With respect to the ice melting envelope, the parametrization reproduced our experimental values to within ±0.37 K; the parametrization of Braban et al.[15] for the ice melting envelope reproduced our data to within ±0.50 K. Braban et al.[15] did not report specific values for their data points in this region; instead, they reported parameter values. From their Figure 5, they apparently measured four points on the ice melting envelope. We interpolated the composition of these points from their figure and calculated the temperatures from their parametrization. Our parametrization reproduced these points to within ±0.12 K (they did not report the accuracy for their parametrization reproducing their own data). Because we have many more data points (22) for the ice melting envelope, and our parametrization reproduces our data and that of Braban et al.[15] well within experimental error, we recommend using our parametrization to calculate the ice melting envelope in the malonic acid/water system. Parameter values are given in Table 2.

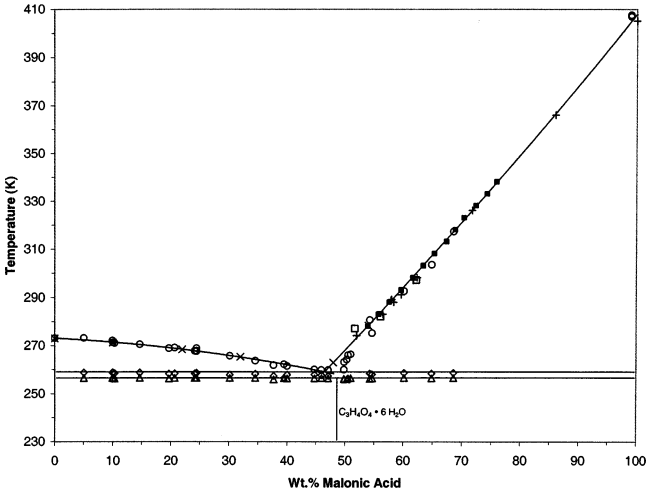

Figure 1. Phase diagram of the $C_3H_4O_4/H_2O$ binary system. Data points from our experiments are as follow: (○) final melting, (◇) eutectic melting, and (△) malonic acid hexahydrate (MAH) thermal decomposition. Literature values for bulk solutions are as follow: (+) Timmermans,[13] (■) Apelblat and Manzurola,[14] (□) Brooks et al.,[8] and (×) Braban et al.[15] Solid/liquid equilibrium lines are fits to the data as given in the text.

For the solid malonic acid/solution equilibrium line, there is a significant amount of literature data to which we can compare our parametrization and that of Braban et al.[15] Although our parametrization for this line reproduced our data well (to within ±1.03 K), its performance in regard to reproducing the literature data was worse (±1.94 K) than the parametrization of Braban et al.[15] (±1.05 K). We feel this phenomenon is because there is a greater uncertainty in our final melting points in this region because of the small thermal signal that is due to the dissolution of solid malonic acid in our samples as the temperature is increased (see Figure 2). The smaller the slope in the thermogram, the greater the uncertainty in the point where $dq/dT = 0$, where q is the heat flow and T is the sample temperature. This is the "peak" in the thermogram that corresponds to the final melting or, in this case, dissolution of the sample. This problem can be addressed by increasing the heating rates, which, in turn, increases peak heights. However, we did not perform these experiments here because of the abundance of literature data for this transition in the malonic acid/water system, and the need for slow heating rates to discern the other transitions. Therefore, we recommend using the parametrization of Braban et al.[15] for

TABLE 1: Phase Transition Temperatures in the Malonic Acid/Water System,[a] as Determined by Differential Scanning Calorimetry (DSC)

malonic acid concentration (wt %)	malonic acid hydrate thermal decomposition temperature (K)	malonic acid/water eutectic temperature (K)	final melting temperature (K)
5.01	256.65	258.82	273.29
9.97	256.71	258.86	272.15
10.04	256.63	258.84	271.37
10.35	256.38	258.59	271.14
14.68	256.68	258.83	270.58
19.72	256.36	258.37	268.93
20.70	256.63	258.43	269.14
24.16	256.62	258.41	267.78
24.45	256.61	258.69	267.85
24.45	256.63	258.77	268.87
24.45	256.57	258.72	267.73
30.18	256.61		265.75
34.54	256.62		263.76
37.69	255.93		261.90
39.48	256.53		262.26
40.00	256.29		261.47
40.00	256.30		261.55
44.72	256.47		260.15
45.94	256.56		259.89
47.11	256.47		259.82
49.84	256.28		260.06
49.87	256.06		263.16
50.32	256.10		264.18
50.56	256.40		266.06
51.00	256.53		266.45
54.29	256.22	258.46	280.76
54.65	256.47		275.18
60.15	256.64	258.74	292.64
64.87	256.40	258.48	303.58
68.59	256.49	258.70	317.43
average	**256.47 ± 0.20**	**258.66 ± 0.17**	

[a] The horizontal line in the table separates the ice primary phase region from the malonic acid primary phase region. See text for explanation of the missing data for the malonic acid/water eutectic between 30.18 and 51.00 wt %.

TABLE 2: Polynomial Coefficients for the eq 1 Fit of Data for Ice (This Work) and Malonic Acid[15] Ice Melting Envelopes

	A_2	A_1	A_0
ice	−0.0036639	−0.13048	273.15
malonic acid	0.0046	2.11	151.1

the solid malonic acid/solution equilibrium line. The parameter values from Braban et al.[15] are given in Table 2.

Finally, to determine the eutectic temperature and composition, the two equations were solved simultaneously and resulted in a calculated eutectic composition and temperature of 46.50 wt % and 259.16 K, respectively. The experimentally determined value of the ice/malonic acid eutectic temperature was concluded using DSC data of samples whose concentration was several weight percent away from the eutectic composition. The reason for this method is that, as the eutectic composition is approached as a function of composition, the mass of sample melting at the eutectic increases. Thus, the DSC signal due to this transition increases substantially. In the malonic acid/water system, this creates a problem, because there is a transition that is due to a hydrate decomposition at 256.7 K (discussed below) that overlaps with the eutectic signal near the eutectic. Therefore, we only averaged the eutectic onset temperatures of samples in the malonic acid concentration ranges of 5−25 and 55−79 wt %. Using this method, the experimentally determined eutectic temperature is 258.66 ± 0.17 K, which is in good agreement (0.50 K) with the calculated value from the fits to the melting/dissolution data. Although it does not introduce significant error, one should note that Braban et al.[15] included a eutectic temperature of 260 K in their parametrization. Also, Parsons et al.[19] determined the eutectic temperature to be 255.7 K, utilizing their deliquescence temperatures for particles and the ice equilibrium vapor pressure. This is 3 K below our measured value and is readily explained by their observed particle

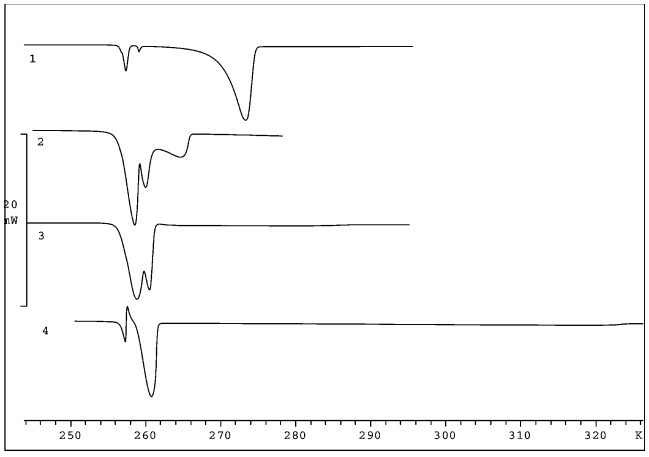

Figure 2. Differential scanning calorimetry (DSC) thermograms of malonic acid/water samples (exotherms point up): (1) 5.01 wt % malonic acid, (2) 30.15 wt % malonic acid, (3) 54.65 wt % malonic acid, and (4) 68.6 wt % malonic acid. For each thermogram the following pattern is followed: the first endotherm is MAH thermal decomposition; the second endotherm is the dissolution of malonic acid, forming a eutectic solution (5.01 and 30.15 wt %), or ice melting to form a eutectic solution (54.65 and 68.6 wt %); and the final endotherm is melting of ice (5.01 and 30.15 wt %) or slow dissolution of malonic acid into the liquid (54.65 and 68.6 wt %, very small and spread over a large temperature range.) In addition, thermogram 4 displays a recrystallization of the liquid at 257 K.

TABLE 3: IR Vibrational Frequencies for Pure Solid Malonic Acid from Two References and Our ATR Experiment, Two Frozen Samples of Malonic Acid/Water, and Malonic Acid Aerosols Dried to 4% Relative Humidity (from Braban et al.[15])

	IR Vibrational Frequency (cm^{-1})					
	Pure Solid Malonic Acid			Frozen Malonic Acid/Water		
mode[25]	ref 25 (303 K)	ref 23	our ATR experiment (298 K)	54.7 wt % (252 K)	51.0 wt % (252 K)	malonic acid aerosol
ν(C═O) (I)	1720	1724	1695	1714	1735	1749[a]
ν(C═O) (II)	1690	1695			1675	1686[a]
$\delta(CH_2)$	1445	1429	1434	1445	1450	1444[b]
δ(OH)	1425	1408	1414	1392		
ν(C−O)	1315	1307	1310	1332	1336	
$\omega(CH_2)$	1225	1217	1215	1234	1228	1229[c]
$t(CH_2)$	1175		1167	1179	1170	
γ(OH)	900	916	893	909	909	
ν_s(C−C)	780	763	767	794		
δ(C−O−O)	660	651	655	669	664	

[a] Braban et al.[15] assigned these modes to the C═O asymmetric and symmetric stretches. [b] Braban et al.[15] assigned this mode to the C−OH bend. [c] Braban et al.[15] assigned this mode to the C−O stretch.

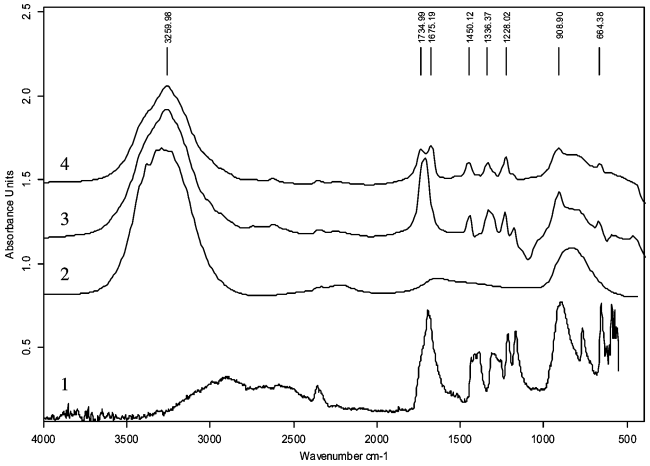

Figure 3. Infrared (IR) spectra of malonic acid/water frozen mixtures: (1) solid malonic acid at 298 K using an ATR accessory (multiplied by a factor of 20, because of the weaker signal compared to other spectra shown); (2) ice at 268 K (divided by 2); (3) frozen 54.7 wt % sample at 252 K, showing characteristics of ice and solid malonic acid; and (4) 51.0 wt % sample at 252 K, showing bifurcation of the peak at 1700 cm^{-1}, characteristic of MAH. Peak values are given for spectrum 4 (MAH) at the top of the figure. Spectra are offset for clarity.

deliquescence temperatures below the liquidus line for bulk solutions. (See discussion on aerosol experiments below.)

3.2. Malonic Acid Hydrate. We have observed evidence of a new solid in both DSC and IR spectroscopy experiments. We observed an exothermic transition in DSC experiments at 256.47 ± 0.20 K in all aqueous samples on heating. Figure 2 shows typical DSC thermograms over a wide concentration range that displayed this transition. The transition occurs at a temperature below the ice/malonic acid eutectic temperature and, thus, does not intersect with either the ice melting envelope or the malonic acid dissolution boundary. Therefore, this transition does not seem to correspond to a eutectic or peritectic transition. Instead, this transition falls into one of three categories: a solid−solid phase transition of either malonic acid or ice, a solid−solid reaction of a new malonic acid/water solid to form a solid solution of ice/malonic acid, or the thermal decomposition of a new malonic acid/water solid to a liquid that does not recrystallize. We are able to rule out the possibility of the observed transition being a solid−solid transition. The properties of ice are well-known and no solid−solid transition has been reported at this temperature and pressure.[30] The thermodynamic properties of solid malonic acid have been studied, and only two solid−solid transitions were observed, at 47.3 and 352.2 K.[11,12] This leaves the conclusion that the observed transition is due to the conversion of a previously unknown malonic acid hydrate to either a solid solution of ice/malonic acid or a liquid. While the latter case appears to always occur in our thermograms, for $[C_3H_4O_4]$ > 56 wt % recrystallization of the melt was observed. Thus, it appears the hydrate decomposes thermally to the liquid rather than undergoing a solid−solid reaction to form a solid solution of ice and solid malonic acid. In cases where the liquid is particularly unstable ($[C_3H_4O_4]$ > 56 wt %), a recrystallization occurs, forming the stable solids. An example thermogram for this case is given in Figure 2.

Our IR spectroscopy experiments also provide evidence for this new solid. Figure 3 shows several spectra, including pure solid malonic acid using an ATR accessory, water-ice, and frozen 51.0 wt % malonic acid and frozen 54.7 wt % malonic acid, each at 252 K. The band assignments for solid malonic acid have been made by Pigenet et al.[24] and Ganguly et al.[25] In Table 3, we list the major spectral bands for solid malonic acid observed by Ganguly et al.,[25] Pouchert,[23] and our work using an ATR accessory. Also listed in the table are the observed bands that correspond to those of solid malonic acid from the two frozen samples shown in Figure 3 and those listed by Braban et al.[15] for malonic acid aerosols dried to 4% relative humidity. Both Pigenet et al.[24] and Ganguly et al.[25] observed a splitting of the C═O stretching peak at ∼1700 cm^{-1}. Ganguly et al.[25] interpreted the splitting to be due to unequal dimer rings in the crystal structure (designated as I and II in Table 3), and they found that the splitting disappeared at temperatures of 360 K and above, where they discerned a solid−solid phase transition from DSC experiments. The spectra of both Pigenet et al.[24] and Ganguly et al.[25] demonstrate a narrow splitting (50 cm^{-1} at 100 K, and 30 cm^{-1} at 303 K, respectively). A comparable splitting is observed in the spectrum of Pouchert,[23] with an even smaller intensity. The splitting of the C═O peak is so small as to not be quantifiable in our solid malonic acid experiments utilizing the ATR accessory. However, Braban et al.[15] observed a very significant bifurcation of the C═O peak in their aerosol spectrum at 4% relative humidity, with a splitting of 63 cm^{-1}. Although we did not observe this splitting for pure malonic acid or any of its aqueous solutions, we did observe a bifurcation of the C═O peak at temperatures of <257 K for $[C_2H_4O_4]$ < 52 wt %, as shown in Figure 3, which corresponds to the hydrate phase transition temperature observed in our DSC experiments.

We have performed several analyses on the IR spectra of frozen malonic acid/water samples to determine if the sample

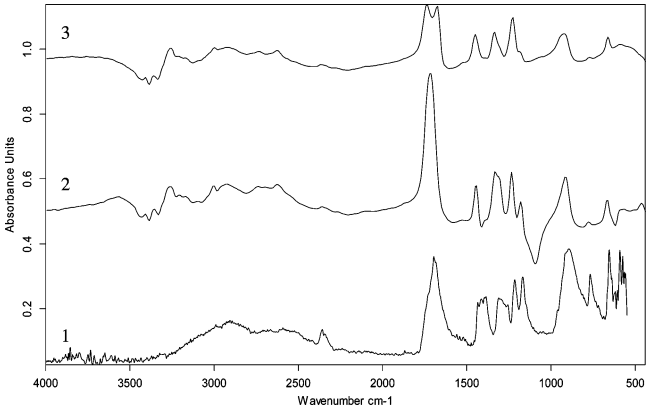

Figure 4. IR spectra of various malonic acid samples: (1) solid malonic acid using an ATR accessory (spectrum is multiplied by 10); (2) difference spectra for the frozen 54.7 wt % malonic acid sample in Figure 3, with the ice spectrum subtracted; and (3) difference spectra for the frozen 51.0 wt % malonic acid sample in Figure 3, with the ice spectrum subtracted. Spectra have been offset for clarity. See text for the subtraction method.

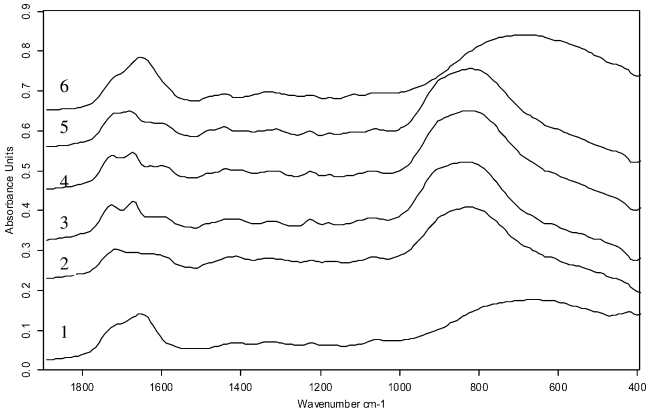

Figure 5. Evolution of 10.0 wt % malonic acid thin film IR spectra with temperature. Cooling: (1) 287 K (liquid), (2) 247 K (ice formation), and (3) 233 K (MAH formation). Warming: (4) 256 K (MAH just before melting), (5) 260 K (MAH melted, but ice still present), and (6) 274 K (ice melted, sample completely liquid). Spectra are offset for clarity.

is simply a mixture of ice and malonic acid or if we can identify a spectral signature that corresponds to the 256.5 K transition in the DSC experiments. In Figure 4, we show the results of spectral subtraction of our ice spectrum from each of the 54.7 and 51.0 wt % spectra (Figure 3), as well as our solid malonic acid spectrum for reference. The spectral subtractions were performed by increasing the amount of the ice spectrum subtracted until the OH peak at 3000 cm^{-1} had dropped to the baseline. It is readily seen that the remaining spectral features in the 54.7 wt % malonic acid sample are very similar to those of solid malonic acid. However, for the 51.0 wt % malonic acid sample, the bifurcation at 1700 cm^{-1} does not disappear but rather remains as substantial as before subtraction. Comparing the vibrational frequencies in Table 3, the following observations are made regarding our frozen 51 wt % malonic acid sample:

(1) Ganguly et al.[25] and Pigenet et al.[24] demonstrated that the splitting of the C═O band increases as the temperature decreases. However, the splitting in our spectrum is greater for a sample at 252 K than that of Pigenet et al.[24] at 100 K.

(2) The δ(OH) mode is missing completely from our spectrum, whereas essentially all the remaining major modes are shifted to higher frequencies than those for solid malonic acid.

(3) We consistently observe the conversion of the C═O bifurcated peak to a single peak at ∼257 K when warming our frozen samples with $[C_2H_4O_4] < 52$ wt %, which corresponds to the transition temperature of the hydrate in the DSC experiments. The strong doublet feature at 1700 cm^{-1} was present in all of these samples, and we observed very little variation in the absorption frequencies. However, the bifurcation was not observed at higher concentrations. This is in agreement with the DSC data that show only a small amount of mass in the hydrate phase at higher concentrations; thus, we would not expect to detect its signature in the IR measurements.

(4) In some cases, samples were frozen into a mixture of water ice and malonic acid and the doublet feature appeared later on further cooling. Other samples were frozen directly into the hydrate spectra.

As a result of these observations and analyses, we conclude that spectrum 4 of Figure 3 represents a unique signature for the malonic acid hydrate. Figure 5 displays IR spectra that correspond to the warming and cooling run of a 10.0 wt % sample. Here, we demonstrate the crystallization of ice, followed by the formation of the hydrate on cooling. During the warming cycle, the hydrate then melts at 257 K, followed by the slow melting of ice, with the final melt corresponding to the phase diagram. In all cases, after the hydrate melts, the sample spectra were always a mixture of aqueous malonic acid and water ice that melted at the appropriate temperature (on the left side of the eutectic). We are not able to regulate the thickness of our films precisely; therefore, we cannot determine accurately if the strength of the hydrate peaks were concentration dependent.

We have tentatively assigned the transition at 256.5 K detected in both DSC and IR experiments to the thermal decomposition of malonic acid hexahydrate ($C_3H_4O_4 \cdot 6H_2O$, MAH). In the DSC experiments, this hydrate is present in all malonic acid/water samples. DSC samples with a malonic acid concentration of 50−51 wt % had the largest energy for this transition and, thus, have the largest amount of the hydrate present in the sample. A composition of $C_3H_4O_4 \cdot 6H_2O$ corresponds to a concentration of 49.05 wt %. A vertical line has been drawn in Figure 2 at this composition.

3.3. Content of the Solid Phase. In a simple binary system where the only stable solid phases are the pure molecular solids that are mixed to make the system, the amount of sample in each solid in a completely frozen sample can be calculated by the lever rule. However, when the possibility of a third, stable molecular solid is introduced, the lever rule predictions likely will not be accurate for the empirical observations, except under conditions of complete equilibrium. This is a condition that is not met either in our experiments or in atmospheric droplets, because of significant supercooling below the equilibrium freezing envelope over a wide range of concentrations. For example, referring to Figure 1, in the concentration range of $0 < [C_3H_4O_4] < 49$ wt % and for $T < 256.5$ K, the only stable phases are predicted to be ice and MAH. However, all DSC samples in this range displayed signals in the DSC experiments corresponding to ice, MAH, and solid malonic acid (where the solid malonic acid did not form from recrystallization of MAH on warming). Therefore, other methods must be used to determine the content of the solid phase from the experimental data.

We have quantitatively determined the amount of solid in each phase for a completely frozen sample using the fusion enthalpies of all but one solid present. The fusion enthalpy of ice is readily known;[31] however, that of solid malonic acid has not previously been measured. Therefore, we used DSC to

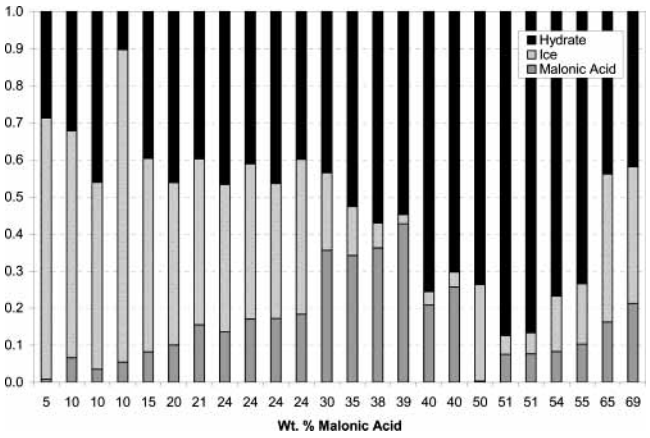

Figure 6. Content of frozen samples expressed as the mass fraction in each solid phase. Each column along the ***x***-axis represents a single sample with the concentration given.

determine the enthalpy of fusion of 99%+ malonic acid, which we found to be 23.1 ± 1.2 kJ/mol. This value is an average from five trials. Using the enthalpy of fusion of water-ice and solid malonic acid, we were able to calculate the mass fraction of each solid in any particular sample; the fraction remaining was assumed to be MAH. This relies on the assumption that the samples are completely frozen. We were able to determine whether samples were completely frozen based on the shape of the first melting endotherm in the DSC thermogram. In all cases, we did not observe indications that samples were not completely frozen. The mass fraction of each solid in a sample (for which fusion enthalpies are known) was calculated using the following equation:

$$y_i = \frac{EM_i}{\Delta H_i^{\mathrm{fus}} m_{\mathrm{T}}} \tag{2}$$

where y_i is the mass fraction of species i (where i represents water ice or solid malonic acid), E the energy of the transition (as measured by DSC), M_i the molar mass of solid i, $\Delta H_i^{\mathrm{fus}}$ the molar enthalpy of fusion of species i, and m_{T} the total mass of the sample. After the mass fractions of ice and solid malonic acid were calculated, the remaining mass fraction in each sample was assigned to MAH. Figure 6 shows the fraction of each solid present by mass in a frozen sample plotted as a function of weight percent. Note that, in some cases, there are multiple samples of a single concentration.

As expected, ice is the major phase at low concentrations (5−15 wt %). At concentrations of 20−25 wt %, the mass fraction of ice and MAH are approximately equal, whereas that of solid malonic acid increases, but is the least of the three. For malonic acid concentrations of 30−55 wt %, MAH is the major phase, and, for solutions of 51 wt % malonic acid, MAH is ∼90% of the solid by mass. In the 30−55 wt % malonic acid range, ice is a very small fraction of the mass (generally <10%). Solid malonic acid represents ∼30% of the mass in the 30−39 wt % range before decreasing to lower values at higher concentrations. We are unclear why the presence of solid malonic acid is enhanced in this small range. At the higher concentrations that we studied (65 and 69 wt %), the amount of MAH present decreases whereas the presence of ice and malonic acid increases. (We did not attempt to study even higher concentrations in the DSC, because these solutions would have had ever increasing malonic acid dissolution temperatures, which would have led to significant evaporation of water from the sample, thus creating a solution of unknown concentration.) The 65 and 69 wt % samples also show a recrystallization of MAH to ice and malonic acid, which is a phenomenon that is not observed in other samples (see Figure 2). However, because the thermal decomposition of MAH is very close in temperature to the eutectic, any ice that forms immediately melts at the eutectic.

Utilizing the mass fraction of MAH, an enthalpy of fusion can be calculated for the thermal decomposition of the hydrate via a rearrangement of eq 2. An average of all samples that contained a MAH mass fraction of at least 0.25 (22, with the exception of the 65 and 69 wt % samples, which had interference from recrystallization peaks) yielded an enthalpy of fusion of 40 ± 13 kJ/mol. The low precision of the calculated value is due to the overlapping of endothermic melting peaks in the thermograms for some samples, which leads to uncertainty in the transition energies.

3.4. Heat Capacity. We have measured constant pressure heat capacities for 5−55 wt % malonic acid/water solutions from 323 K to the respective freezing point of each solution. Specific heat capacities (in units of J g^{-1} K^{-1}) are given as a function of temperature and solution concentration in Table 4. For reference, we also measured the constant pressure heat capacity of HPLC grade water that was supplied by Aldrich. On comparison with literature values[32] in the temperature range of 273−315 K, we found our values to be within 1.15% of the literature values. This is better than the 2% accuracy determined using the Mettler-Toledo DSC studying various chemical systems.[33] The general trend in our data is decreasing heat capacity with decreasing temperature, regardless of concentration, with the exception of the 35 wt % sample. It is unclear why this is the case. We repeated the 35 wt % experiments several times, with no significant change in the heat capacity results. For the concentration range of 5−15 wt %, the heat capacity values change significantly with concentration. However, at higher concentrations, the heat capacity values begin to cluster between 3.5 and 4.5 J g^{-1} K^{-1}. For the concentrations 35−55 wt %, the heat capacity values are essentially the same, within experimental error. Heat capacity measurements at 303 K have been performed by Kawaizumi et al.[20] for $[C_2H_4O_4]$ < 0.18 wt %; thus, there is no point of comparison between their data and that presented here. At these low concentrations, Kawaizumi et al.[20] determined that the solution heat capacities were very similar to that of water.

3.5. Water Activities. In a simple binary system, the freezing point depression can be used to determine solvent activities via the equation

$$\ln a_i = -\int_{T_{\mathrm{f}}}^{T_{\mathrm{f}}^*} \frac{\Delta H_{\mathrm{f}}}{RT^2}\,\mathrm{d}T \tag{3}$$

where a_1 is the activity of water at T_{f}, ΔH_{f} is the molar enthalpy of fusion of ice, R = 8.314 J mol^{-1} K^{-1}, T_{f} is the depressed melting point, and T_{f}^* is the melting point of pure water. To a first approximation, the enthalpy of fusion can be considered constant as a function of temperature over a small temperature range, and then eq 3 is simply

$$\ln a_1 = \frac{\Delta H_{\mathrm{f}}}{R}\left(\frac{1}{T_{\mathrm{f}}^*} - \frac{1}{T_{\mathrm{f}}}\right) \tag{4}$$

We have determined the water activities of our solutions at T_{f} in the range of the ice melting envelope, 0 wt % < $[C_3H_4O_4]$ < 48 wt %. From this, water activity coefficients (γ_1) are calculated using $a_1 = \gamma_1 x_1$, with x_1 being the mole fraction of

TABLE 4: Constant Pressure Specific Heat Capacity Values for Malonic Acid/Water Solutions as a Function of Temperature and Concentration

	Constant Pressure Specific Heat Capacity (J g^{-1} K^{-1})										
temperature, T (K)	5.04 wt %	9.58 wt %	14.92 wt %	20.00 wt %	24.40 wt %	30.16 wt %	34.96 wt %	39.98 wt %	44.40 wt %	49.02 wt %	55.37 wt %
323	6.09	5.69	5.09	4.71	4.68	4.25	3.91	4.04	3.87	3.74	3.84
321	6.11	5.71	5.09	4.70	4.68	4.25	3.91	4.04	3.87	3.74	3.85
319	6.11	5.71	5.08	4.69	4.69	4.24	3.90	4.04	3.86	3.73	3.84
317	6.12	5.72	5.08	4.67	4.69	4.24	3.89	4.04	3.86	3.72	3.84
315	6.11	5.71	5.06	4.66	4.68	4.23	3.88	4.05	3.85	3.71	3.83
313	6.10	5.70	5.05	4.65	4.67	4.21	3.86	4.05	3.84	3.69	3.82
311	6.10	5.69	5.04	4.64	4.66	4.20	3.84	4.06	3.82	3.68	3.81
309	6.11	5.69	5.03	4.64	4.66	4.19	3.82	4.08	3.82	3.67	3.80
307	6.11	5.68	5.03	4.62	4.65	4.16	3.81	4.08	3.81	3.66	3.80
305	6.11	5.67	5.02	4.61	4.64	4.15	3.81	4.09	3.80	3.65	3.79
303	6.10	5.67	5.02	4.61	4.64	4.15	3.80	4.09	3.79	3.64	3.78
301	6.10	5.66	5.01	4.60	4.63	4.14	3.79	4.09	3.78	3.63	3.77
299	6.09	5.64	5.01	4.60	4.62	4.14	3.79	4.09	3.77	3.63	3.76
297	6.03	5.57	4.96	4.54	4.56	4.09	3.74	4.04	3.72	3.58	3.71
295	6.02	5.55	4.95	4.53	4.54	4.08	3.73	4.04	3.70	3.57	3.69
293	6.01	5.53	4.94	4.52	4.53	4.08	3.72	4.04	3.69	3.55	3.68
291	6.01	5.52	4.92	4.51	4.52	4.07	3.71	4.04	3.68	3.54	3.67
289	6.02	5.52	4.91	4.50	4.51	4.05	3.70	4.03	3.67	3.53	3.66
287	6.02	5.50	4.89	4.48	4.50	4.04	3.69	4.02	3.66	3.52	3.65
285	6.00	5.50	4.87	4.47	4.49	4.02	3.68	4.01	3.65	3.52	3.64
283	5.98	5.49	4.86	4.46	4.48	4.01	3.67	4.00	3.65	3.52	3.64
281	5.97	5.47	4.85	4.46	4.48	4.01	3.67	3.99	3.64	3.52	3.63
279	5.95	5.48	4.85	4.45	4.48	4.00	3.67	3.99	3.64	3.51	3.63
277	5.95	5.50	4.84	4.45	4.48	4.00	3.66	3.98	3.63	3.51	3.63
275	5.94	5.51	4.83	4.44	4.47	3.99	3.65	3.98	3.64	3.51	3.63
273	5.92	5.49	4.82	4.44	4.47	3.99	3.66	3.98	3.64	3.52	3.63
271	5.91	5.47	4.81	4.43	4.47	3.99	3.65	3.97	3.63	3.52	3.61
269	5.90	5.46	4.81	4.42	4.47	3.99	3.63	3.96	3.62	3.51	3.60
267	5.90	5.45	4.8	4.41	4.46	3.97	3.62	3.95	3.61	3.50	3.59
265	5.89	5.43	4.79	4.40	4.44	3.96	3.60	3.93	3.60	3.49	3.57
263	5.87	5.41	4.77	4.38	4.41	3.93	3.58	3.91	3.58	3.47	3.55
261	5.87	5.39	4.75	4.37	4.39	3.91	3.57	3.89	3.56	3.46	3.53
259	5.86	5.38	4.75	4.37	4.38	3.89	3.55	3.89	3.55	3.45	3.52
257	5.86	5.37	4.74	4.37	4.37	3.89	3.55	3.89	3.54	3.44	3.51
255		5.37			4.36	3.88	3.54	3.89	3.53	3.43	3.50
253					4.35	3.87	3.53	3.88	3.52	3.43	3.50
251						3.86	3.52	3.86	3.51	3.42	3.48
249						3.85	3.51	3.85	3.50	3.41	3.48
247							3.51	3.83	3.50	3.40	3.47
245								3.81	3.49	3.40	3.46
243									3.48	3.39	3.45
241									3.47	3.38	3.44
239										3.37	3.43
237										3.36	3.41
235										3.35	3.40
233										3.34	3.39
231											3.36

water. Within experimental error, the water activity coefficient was calculated to be unity at T_f over the concentration range of our experiments. Utilizing the parametrizations of Braban et al.[15] for bulk solutions of constant relative humidity as a function of temperature, and values for the solid/liquid equilibrium boundary, the activity coefficients at T_f can be calculated for their experiments. The results are given in Figure 7, along with values from our experiments and those of Brooks et al.[8] at three temperatures; the figure shows that the data are in excellent agreement. Braban et al.[15] also determined solution activities as a function of temperature and concentration. We have plotted γ_1 for their data at 293.3 K. For $a_1 > 0.85$, γ_1 is independent of temperature (same values at 293.3 K as at T_f); however, at lower water concentrations, γ_1 decreases as the temperature increases. Peng et al.[16] used an electrodynamic balance for single particles and vapor pressure measurements of bulk solutions to measure water activities as a function of mole fraction of solute for malonic acid/water samples at 298 K. Both data sets are in excellent agreement with our data and that of Braban et al.[15] In all of these data sets, the solution is essentially ideal for $a_1 > 0.88$, and, at lower activities, γ_1 appears to decrease monotonically with a_1. Wise et al.[18] also measured water vapor pressures over bulk solutions at 298 K. However, in their interpretation of the data, their γ_1 values decrease linearly with water mole fraction x_1 and do not show an approach to ideal conditions at $a_1 = 0.88$. Because the experiments of Wise et al.[18] are similar to the constant temperature bulk measurements of Braban et al.[15] and Peng et al.,[16] we do not have an explanation for why their data would show such a deviation. Close inspection of the data shown in Figure 2a of their paper shows the possibility of interpreting their results more in line with the results of other experiments: the data could be interpreted as showing that malonic acid solutions are ideal up to a water mole fraction of $x_1 = 0.91$.

3.6. Comparison with Aerosol Experiments. Many researchers have determined the deliquescence and efflorescence relative humidities of malonic acid/water aerosols using various

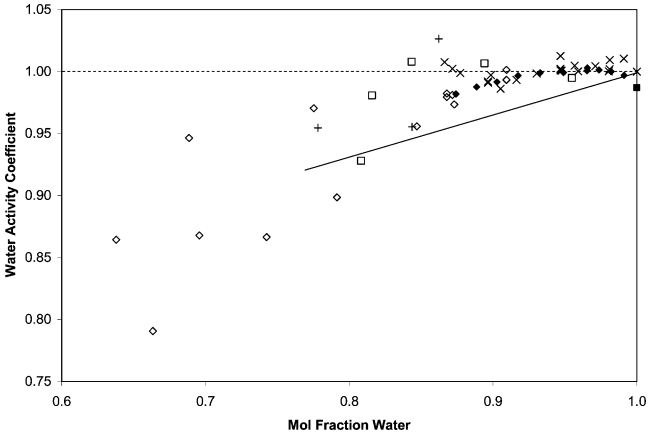

Figure 7. Plot of water activity coefficient as a function of water activity: (×) determined by freezing point depression (this work); (◇) single particle electrodynamic balance experiments at 298 K, from Peng et al.;[16] (◆) bulk relative humidity measurements at 298 K, from Peng et al.;[16] (□) calculated bulk relative humidity measurements following the liquidus line, from Braban et al.;[15] (■) values from bulk relative humidity measurements at 293.1 K, from Braban et al.;[15] (+) relative humidity measurements at T_f over bulk solutions, from Brooks et al.;[8] and the solid line is water vapor pressure measurements over bulk solutions at 298 K, from Wise et al.[18] Dashed line represents an ideal solution ($\gamma_1 = 1$).

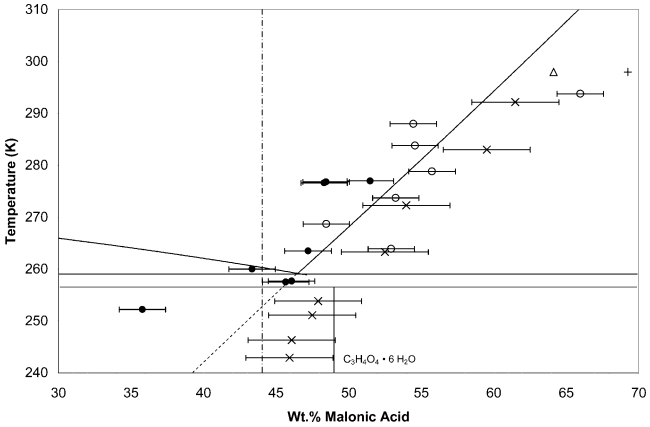

Figure 8. Plot of literature data for deliquescence relative humidities (DRHs) converted to solution concentrations (using the method given in the text) on the malonic acid/water solid/liquid phase diagram (dashed line is an extension of the malonic acid liquidus line): (○) Braban et al.,[15] aerosol flow tube experiments; (●) Braban et al.,[15] static mode chamber experiments (error bars represent ±1.6 wt %; see text); (△) Prenni et al.,[17] calculated value; (+) Peng et al.;[16] and (×) Parsons et al.[19] (error bars represent ±3 wt %; see text). Vertical dashed−dotted line indicates the concentration at which solutions become ideal ($[C_3H_4O_4] < 44.1$ wt %).

techniques as a function of temperature, including methods that involve a single particle in an electrodynamic balance (Peng et al.[16]), a differential mobility analyzer (Prenni et al.[17]), a flow tube and static mode chamber (Braban et al.[15]), and microscopy of aerosols deposited on a hydrophobic surface (Parsons et al.[19]). To compare the results of these studies to the phase diagram, one must know the activity coefficients to determine the mole fraction or mass fraction of solute from the solution activities (deliquescence relative humidities, DRHs). As given in the previous section, for $a_1 > 0.88$ ($[C_3H_4O_4] > 44.1$ wt %), the malonic acid/water solutions are essentially ideal and $a_1 = x_1$. For lower water content, we parametrized the bulk data from Braban et al.,[15] Brooks et al.,[8] our work, and the bulk and aerosol data of Peng et al.[16] for $0.55 < a_1 < 0.90$, which resulted in the equation $\gamma_1 = 0.4079a_1 + 0.6401$. At $a_1 < 0.55$, only Peng et al.[16] have measured water activities, and γ_1 appears to increase as a_1 decreases. Therefore, using the aforementioned equation for γ_1, $[C_3H_4O_4]$ can be calculated for aerosol experiments using DRHs. The results are plotted in Figure 8. None of these studies have reported the observation of solid malonic acid inclusions in deliquesced particles; therefore, deliquescence must be occurring at the malonic acid/solution equilibrium boundary on the phase diagram. However, the calculated aerosol concentrations do not consistently fall on this boundary.

The data of Parsons et al.[19] and Peng et al.[16] are consistently below the liquidus line. Prenni et al.[17] did not observe deliquescence of malonic acid/water aerosols, but they did calculate a DRH at 298 K, which also falls below the liquidus line. Braban et al.[15] plotted their aerosol DRH temperatures and compositions on the phase diagram (Figure 5 in their paper), calculating the concentration of water ($[H_2O]$) in their aerosols from a parametrization of their bulk RH data. The calculation of aerosol concentrations from their DRH values using the activity coefficients calculated here does not give the same $[H_2O]$ values that they calculated. According to our analysis, their data are scattered about the malonic acid liquidus line for static mode aerosol chamber experiments. For aerosol flow tube experiments, their data are either at or above the malonic acid liquidus line. However, the existence of pre-deliquescent aerosols to the left of the liquidus line would be thermodynamically unstable. Much of the discrepancy in calculated concentrations between our analysis and theirs is very likely due to the uncertainty in their parametrization of their bulk data. They state that, for RH > 80%, the model uncertainty is ±1%. This represents an uncertainty in the concentration of ±1.6 wt %; error bars that express this uncertainty are shown for their data in Figure 8. At lower relative humidities, the uncertainty is even greater, ±3% RH (±4.6 wt %). Also, Braban et al.[15] reported many aerosol DRH data points outside the temperature range of their parametrization (274−293 K). These uncertainties, coupled with the uncertainties in our parametrization of the activity coefficient data, likely explain the discrepancies between the two analyses. There is also significant uncertainty in the data of Parsons et al.[19] They reported their uncertainty in the DRH measurements to be ±2.1% RH (±3 wt %), and we have plotted these error bars on their data in Figure 8. However, their values are consistently below the malonic acid liquidus line, which could be explained by a systematic error in either the calculated activity coefficients or the aerosol data. However, should the Parsons et al.[19] data be shifted to lower malonic acid concentrations, because of a systematic error in the activity coefficient data, the data of Braban et al.[15] would also be shifted by this same amount further to the right of the liquidus line, indicating an error of equal magnitude in that data set. A third possible explanation for the differences between the Braban et al.[15] and Parsons et al.[19] data is that deliquescence is kinetically hindered for very small particles. Thus, the smaller aerosols of Braban et al. (0.1−0.2 μm),[34] as compared to those of Parsons et al. (2−40 μm),[19] could lead to deliquescence at higher relative humidities in the Braban et al.[15] experiments, especially for the short time scales of the flow tube experiments. However, we are not aware of experimental evidence that would confirm a kinetic hindrance of deliquescence based on particle size. Our conclusion is that more accurate activity/activity coefficient measurements and aerosol DRH measurements need to be performed to clarify these uncertainties.

We note that Parsons et al.[19] did not see evidence for the MAH at temperatures of <256 K; their dry aerosols simply deliquesced to give supercooled solutions. This is not unexpected, because there clearly will be a barrier to nucleation of

any solid phase. In our DSC experiments, the onset of crystallization did not occur until temperatures had reached 256 K or lower for $[C_3H_4O_4] < 65$ wt %, and near the eutectic composition, crystallization did not occur until 240 K or lower. We would expect nucleation to occur at lower temperatures in aerosols than we observed in our experiments.

Braban et al.,[15] whose lowest observed temperature was 252 K, did not see evidence for crystallization in their aerosol experiments. However, on much longer time scales at low temperatures, such as may occur in the free troposphere, the nucleation of ice, MAH, or malonic acid could occur, depending on the concentration of malonic acid in aerosols and other species present. Thus, the phase diagram represents the equilibrium boundaries when applied to atmospheric aerosols, but it does not determine nucleation probabilities or crystallization kinetics.

4. Summary and Atmospheric Implications

We have investigated the low temperature thermochemical properties of the malonic acid/water system using differential scanning calorimetry (DSC) and infrared (IR) spectroscopy of thin films. Specifically, we conclude:

The solid/liquid phase diagram shows that our results are in excellent agreement with the historic compilation of Timmermans[13] for malonic acid solubilities and the work on bulk solutions by Braban et al.,[15] Apelblat and Manzurola,[14] and Brooks et al.[8] The eutectic concentration and temperature have been experimentally determined directly and indirectly using DSC. Other researchers,[15,19] using indirect methods, have determined values within 3 K of our value. Because of the high temperature accuracy of the DSC technique, we recommend our value as being the closest to true.

We have made the first observations of a malonic acid hydrate. We have observed a substantial endothermic transition when the samples are heated, which we have assigned to be the thermal decomposition of malonic acid hexahydrate (MAH). This transition was observed in both DSC and IR thin film studies, and we have reported a unique IR spectrum that corresponds to this solid. MAH was observed over a large range of concentrations (5 wt % $< [C_3H_4O_4] <$ 69 wt %, the entire range we studied).

We have reported the first measurements of the enthalpy of fusion of malonic acid and MAH. Utilizing fusion enthalpies, the content of the solid phase of our samples has been determined, which could not have been predicted simply using the lever rule. It appears if aqueous upper tropospheric aerosols contain even small amounts of malonic acid, should crystallization occur, MAH is a solid that could form. If MAH has a smaller nucleation barrier than ice and thus forms first, it could potentially serve as a site for heterogeneous nucleation of ice in cirrus clouds.

We have measured the constant pressure heat capacities of solutions of 5−55 wt % malonic acid in the temperature range from 323 K down to the freezing point of each respective solution. We observed that the heat capacities of the solutions decreased as the concentration increased and the temperature decreased.

Utilizing the freezing point depression method, we have determined the water activity of our solutions in the range of the ice melting envelope. Our results are in excellent agreement with the bulk solution and aerosol data of Peng et al.,[16] Brooks et al.,[8] and Braban et al.[15] However, the results of Wise et al.[18] are not in agreement with these. Analysis of our data and that of Peng et al.,[16] Braban et al.,[15] and Brooks et al.[8] shows that malonic acid solutions are essentially ideal for water activities greater than 0.88.

Finally, aerosol studies of Braban et al.[15] demonstrate a deliquescence relative humidity (DRH) near the malonic acid liquidus line; however, aerosol deliquescence reported by Parsons et al.,[19] Peng et al.,[16] and Prenni et al.[17] consistently occurs at $C_3H_4O_4$ concentrations to the right of the malonic acid/solution liquidus line. This observation indicates uncertainty either in the activity/activity coefficient data or in the DRH values measured from aerosol experiments, or both. More accurate studies should be undertaken to measure the concentration and activity of malonic acid solutions as well as malonic acid aerosol DRH values.

Acknowledgment. We are grateful to the following people: J. Abbatt and C. Braban, for many helpful conversations on the malonic acid/water system; A. Bertram, for providing a manuscript of work performed in his lab before publication, as well as raw data from their experiments; and C. Peng, for providing raw data from their experiments. This work was supported by the National Science Foundation Atmospheric Chemistry Program (No. ATM-0304966).

References and Notes

(1) Kawamura, K.; Ikushima, K. *Environ. Sci. Technol.* **1993**, *27*, 2227−2235.
(2) Sheridan, P. J.; Brock, C. A.; Wilson, J. C. *Geophys. Res. Lett.* **1994**, *23*, 2587−2590.
(3) Loflund, M.; Kaser-Giebl, A.; Schuster, B.; Giebl, H.; Hitzenberger, R.; Puxbaum, H. *Atmos. Environ.* **2002**, *36*, 1553−1558.
(4) Tervahattu, H.; Hartonen, K.; Kerminen, V.; Kupiainen, K.; Aarnio, P.; Koskentalo, T.; Tuck, A. F.; Vaida, V. *J. Geophys. Res.* **2002**, *107* (D7), AAC-1.
(5) Murphy, D. M.; Thomson, D. S.; Mahoney, M. J. *Science* **1998**, *282*, 1664−1668.
(6) Saxena, P.; Hildemann, L. M.; McMurry, P. H.; Seinfeld, J. H. *J. Geophys. Res.* **1995**, *100*, 18755−18770.
(7) Choi, M. Y.; Chan, C. K. *Environ. Sci. Technol.* **2002**, *36*, 2422−2428.
(8) Brooks, S. D.; Wise, M. E.; Cushing, M.; Tolbert, M. A. *Geophys. Res. Lett.* **2002**, *29*, 1917.
(9) Tabazadeh, A.; Toon, O. B. *Geophys. Res. Lett.* **1998**, *25*, 1379−1382.
(10) Kawamura, K.; Semere, R.; Imai, Y.; Fujii, Y.; Hayashi, M. *J. Geophys. Res.* **1996**, *101*, 18721−18728.
(11) Petropavlov, N. N.; Tsygankova, I. G.; Teslenko, L. A. *Sov. Phys. Crystallogr.* **1988**, *33*, 853−855.
(12) Fukai, M.; Matsuo, T.; Suga, H. *Thermochim. Acta* **1991**, *183*, 215−243.
(13) Timmermans, J. *The Physicochemical Constants of Binary Systems in Concentrated Solutions*; Interscience: New York, 1960; p 393.
(14) Apelblat, A.; Manzurola, E. *J. Chem. Thermodyn.* **1987**, *19*, 317−320.
(15) Braban, C. F.; Carroll, M. F.; Styler, S. A.; Abbatt, J. P. D. *J. Phys. Chem. A* **2003**, *107*, 6594−6602.
(16) Peng, C.; Chan, M. N.; Chan, C. K. *Environ. Sci. Technol.* **2001**, *35*, 4495−4501.
(17) Prenni, A. J.; DeMott, P. J.; Kreidenweis, S. M.; Sherman, D. E. *J. Phys. Chem. A* **2001**, *105*, 11240−11248.
(18) Wise, M. E.; Surratt, J. D.; Curtis, D. B.; Shilling, J. E.; Tolbert, M. A. *J. Geophys. Res.* **2003**, *108*, 4638 (doi: 10.1029/2003JD003775).
(19) Parsons, M. T.; Mak, J.; Lipetz, S. R.; Bertram, A. K. *J. Geophys. Res.*, in press, **2004**.
(20) Kawaizumi, F.; Noguchi, T.; Miyahara, Y. *Bull. Chem. Soc. Jpn.* **1977**, *50*, 1687−1689.
(21) Zhang, R.; Wooldridge, P. J.; Abbatt, J. P. D.; Molina, M. J. *J. Phys. Chem.* **1993**, *97*, 7351−7358.
(22) Lide D. R., Ed. *CRC Handbook of Chemistry and Physics*, 74th ed.; CRC Press: Boca Raton, FL, 1993; pp 3-208, 3-351, and 6-58.
(23) Pouchert, C. J. *The Aldrich Library of Infrared Spectra*; Aldrich Chemical Co.: Milwaukee, WI, 1981; p 288.
(24) Pigenet, C.; Lucazeau, G.; Novak, A. *J. Chim. Phys.* **1976**, *10*, 141−145.
(25) Ganguly, S.; Fernandes, J. R.; Desiraju, G. R.; Rao, C. N. R. *Chem. Phys. Lett.* **1980**, *69*, 227.

(26) Schubnell, M. *J. Therm. Anal. Calorim.* **2000**, *61*, 91.
(27) Beyer, K. D.; Hansen, A. R. *J. Phys. Chem.* **2002**, *106*, 10275−10284.
(28) Standard Test Method for Determining Specific Heat Capacity by Differential Scanning Calorimetry, ASTM Method E 1269-01; American Society for Testing and Materials: West Conshohocken, PA, 2001; pp 1−6.
(29) Lide, D. R., Ed. *CRC Handbook of Chemistry and Physics*, 74th ed.; CRC Press: Boca Raton, FL, 1993; p 3-311.
(30) Petrenko, V. F.; Whitworth, R. W. *Physics of Ice*; Oxford University Press: Oxford, U.K., 1999; pp 252−286.
(31) Zeleznik, F. J. *J. Phys. Chem. Ref. Data* **1991**, *20*, 1157.
(32) Weast, R. C., Ed. *CRC Handbook of Chemistry and Physics*, 65th ed.; CRC Press: Boca Raton, FL, 1984; p D-175.
(33) Widmann, J. Measuring Specific Heat Capacity. *UserCom* **1998**, *7*, 1.
(34) Abbatt, J. P. D., private communication, 2004.